IJCRT.ORG ISSN : 2320-2882

INTERNATIONAL JOURNAL OF CREATIVE RESEARCH THOUGHTS (IJCRT)

An International Open Access, Peer-reviewed, Refereed Journal

Design of a Novel Snowflake-Inspired Slotted Hexagonal Microstrip Patch Antenna for 28 GHz 5G NR Millimeter-Wave Applications

Mrs. Srividhya N, Sanjai R, Sanjay R, Nithishkumar B, Rajkumar M.

Department of Electronics and Communication Engineering,

K. Ramakrishnan College of Engineering, Trichy, Tamil Nadu, India

Abstract A Snowflake-Inspired Slotted Hexagonal Microstrip Patch Antenna (SSHMPA) incorporating five asymmetric inward-pointing triangular slots over a Rogers RT/duroid 5880 dielectric substrate (er = 2.2, h = 0.254 mm) is presented for millimeter-wave 5G NR operation centered at 28 GHz. Electromagnetic simulation conducted in CST Studio Suite 2025 validates that the introduced asymmetric slot arrangement achieves a -10 dB impedance bandwidth of 2.3 GHz, which is approximately nine times greater than that of the plain hexagonal reference structure. The verified performance figures include a return loss of -11.50 dB, a voltage standing wave ratio of 1.724, a realized gain of 5.28 dBi, and a radiation efficiency value of 86.9 percent at the resonant point of 27.94 GHz.

Keywords Snowflake slot antenna, Hexagonal patch, 28 GHz mmWave, 5G NR, Multi-mode resonance, Bandwidth widening, CST simulation, Impedance matching, Slot loading

1. Introduction

Millimeter-wave spectrum utilization has become central to meeting the escalating throughput demands of next-generation wireless infrastructure. Among the frequency allocations identified for fifth-generation deployment, the 28 GHz region — catalogued under 3GPP band designation n257 — has emerged as a primary choice for fixed wireless access and mobile broadband owing to its combination of available spectrum width and manageable propagation characteristics [1]. Network operators deploying infrastructure at this frequency require radiating elements that can sustain continuous operation over the full 3GPP-specified allocation spanning 26.5 to 29.5 GHz, a requirement that immediately disqualifies conventional narrowband antenna configurations [2].

Planar patch radiators have long been favored in integrated wireless hardware owing to characteristics that include minimal volumetric profile, straightforward photolithographic fabrication, and natural compatibility with feeding network implementation on the same substrate layer [3]. Within the family of patch geometries, the hexagonal configuration occupies a position of particular electromagnetic interest: its six-fold rotational symmetry yields a more isotropic current distribution across the patch surface compared to rectangular forms of equivalent resonant dimensions, and the larger radiating perimeter-to-area ratio can theoretically support improved coupling to the surrounding medium. Despite these inherent geometric merits, hexagonal patch structures operating without modification exhibit a pronounced single-mode resonance characterized by a high quality factor that confines their useful impedance bandwidth to a narrow window around the resonant frequency — typically spanning only a few hundred megahertz — which falls well short of practical 5G NR system requirements [4].

Etching strategically dimensioned apertures into the conducting surface of a patch antenna is a recognized approach for redistributing surface currents and introducing secondary resonance phenomena in the vicinity of the fundamental mode. When multiple such apertures are arranged with deliberate geometric asymmetry, the resulting perturbations produce a set of closely clustered resonance poles whose collective effect is a substantially broadened impedance response [5]. Literature documents the application of several aperture forms — including rectangular U-shaped notches, cross-slot configurations, and iterative fractal apertures — for bandwidth widening in patch structures operating below 10 GHz [6]. Extension of this principle to millimeter-wave hexagonal patch geometries at 28 GHz, and in particular the application of a snowflake-inspired triangular slot arrangement to such structures, has not been documented in prior published work.

This study introduces an original antenna geometry designated the Snowflake-Inspired Slotted Hexagonal Microstrip Patch Antenna (SSHMPA), constructed by etching five triangular apertures at the edges of a hexagonal patch in a pattern that approximates the branching geometry of natural snowflake crystal formations. A sixth aperture at the feed-side edge is intentionally omitted to preserve feed line continuity and to break the otherwise perfect hexagonal symmetry, which produces a distinct impedance modification effect. The structure is constructed on Rogers RT/duroid 5880 substrate and characterized through full-wave time-domain simulation in CST Studio Suite 2025. Verified outcomes include a -10 dB bandwidth of 2.3 GHz at a center resonance of 27.94 GHz, representing a ninefold expansion relative to the unmodified hexagonal reference, alongside satisfactory return loss, standing wave ratio, gain, and efficiency values.

A detailed account of the design methodology is presented in Section 2, covering layer-by-layer construction steps with complete dimensional specifications. Section 3 delivers a thorough analysis of simulation results encompassing return loss, standing wave ratio, far-field patterns, gain, near-field distributions, and surface current behaviour. Comparative evaluations against both the unslotted reference and previously reported 28 GHz configurations are included. Concluding observations are provided in Section 4.

2. Antenna Design and Configuration

2.1 Antenna Geometry and Structure

Three distinct conducting and dielectric layers constitute the complete SSHMPA assembly as depicted in Fig. 1. At the base of the stack sits a full-coverage copper ground layer with lateral dimensions of 15 mm by 15 mm and a thickness corresponding to standard one-ounce copper foil at 0.035 mm. Immediately above this ground layer, Rogers RT/duroid 5880 dielectric material fills a slab of identical lateral extent with a thickness of 0.254 mm, equivalent to the commercial 10-mil sheet specification. This substrate variant was selected for its well-documented millimeter-wave performance attributes: a relative permittivity of 2.2 with minimal frequency dependence across the mmWave range and a dissipation factor of 0.0009, among the lowest commercially available values. The uppermost layer carries the radiating element — a hexagonal copper patch of side length 4.55 mm bearing five triangular apertures — connected to a 50-ohm microstrip transmission line oriented along the negative Y-axis.

Each of the five triangular apertures carries dimensions of 1.40 mm in length and 0.35 mm at the base, positioned with their apex pointing inward at a radial offset of 1.20 mm from the geometric center of the hexagon. Aperture 1 occupies the top edge of the hexagon. Apertures 2 and 3 are located at the lower-left and lower-right edge pairs respectively, displaced by 120 and 240 degrees from Aperture 1. Apertures 4 and 5 are sited at the upper-left and upper-right edges at 60 and 300 degrees. The bottom edge, which coincides with the feed attachment point, carries no aperture. This asymmetric arrangement of five rather than six slots is the structural feature responsible for the multi-mode impedance response. All geometric parameters are collected in Table 1.

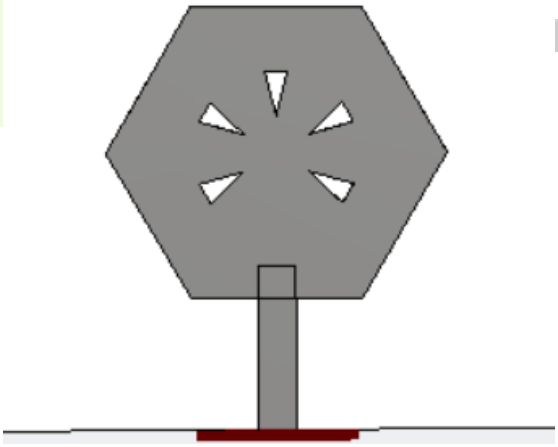

a)

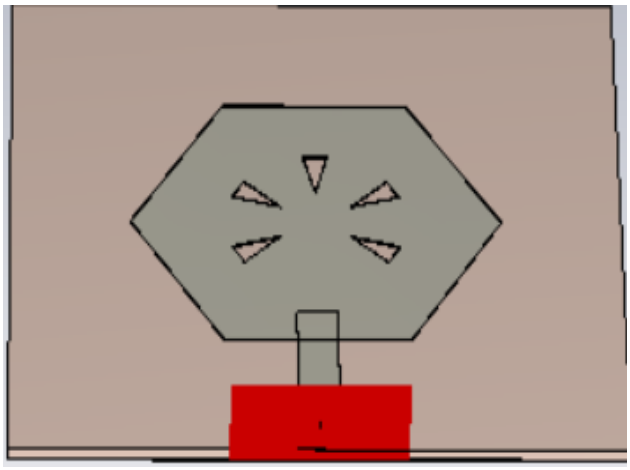

b)

Figure 1. Configuration of the proposed SSHMPA: (a) Top view showing snowflake-inspired five-slot hexagonal patch, (b) 3D isometric view with ground plane, substrate, patch, and microstrip feed line

The complete dimensional summary covering all structural parameters of the proposed SSHMPA is presented in Table 1 below for reference during fabrication and simulation replication.

Table 1. Complete design parameters of the proposed SSHMPA

Parameter	Symbol	Value	Unit
Substrate Length	Lsub	15.0	mm
Substrate Width	Wsub	15.0	mm
Substrate Height	h	0.254	mm
Relative Permittivity	εr	2.2	—
Loss Tangent	tan δ	0.0009	—
Hex Side Length	a	4.55	mm
Ground Plane Size	Lg × Wg	15 × 15	mm
Copper Thickness	t	0.035	mm
Feed Line Width	Wf	0.50	mm
Feed Line Length	Lf	4.469	mm
Slot Length	Ls	1.40	mm
Slot Width	Ws	0.35	mm
Slot Offset	ds	1.20	mm
Number of Slots	N	5	—

2.2 Mathematical Design Equations

Preliminary sizing of the hexagonal patch follows the established resonance relation for the TM10 excitation mode. Expressing the resonant frequency in terms of the side length yields equation (1) below, where the free-space propagation speed c is taken as 3 x 10^8 m/s and ereff denotes the effective substrate permittivity evaluated at the patch width:

$$fr = (1.154 \times c) / (a \times \sqrt{\varepsilon reff}) \quad ...(1)$$

The effective permittivity accounting for lateral field fringing is obtained from equation (2), where er is the substrate relative permittivity, h is the substrate thickness, and W represents the effective patch width dimension:

$$\varepsilon reff = (\varepsilon r + 1)/2 + (\varepsilon r - 1)/2 \times (1 + 12h/W)^{(-0.5)} \quad ...(2)$$

Inserting er = 2.2 and h = 0.254 mm into equation (2) yields ereff = 2.06. Back-substituting into equation (1) at a target frequency of 28 GHz produces an initial side length estimate of 8.6 mm. Correction for the compressive effect of the dielectric medium on the effective wavelength, combined with iterative parametric refinement within CST, converges to a final side dimension of a = 4.55 mm.

The 50-ohm feed line geometry is derived from the standard closed-form microstrip impedance expressions in equations (3) and (4):

$$Z0 = (60/\sqrt{\varepsilon reff}) \times \ln(8h/Wf + Wf/4h), \text{ for } Wf/h \leq 1 \quad ...(3)$$

$$Z0 = (120\pi) / [\sqrt{\varepsilon reff} \times (Wf/h + 1.393 + 0.667 \times \ln(Wf/h + 1.444))], \text{ for } Wf/h > 1 \quad ...(4)$$

Solving for a target impedance of 50 ohms with the given substrate parameters produces a feed conductor width of Wf = 0.50 mm. The feed length of Lf = 4.469 mm is determined to satisfy a quarter-guided-wavelength transformer condition at 28 GHz, ensuring direct conjugate impedance match at the patch boundary.

2.3 Step-by-Step CST Design Procedure

The antenna model is assembled within CST Studio Suite 2025 following the six-step sequence outlined below. Each step is accompanied by the corresponding simulation workspace screenshot for verification.

Step 1 — Ground Plane Construction:

Using the Brick primitive under the Modeling tab, the ground conductor is created by specifying X from -7.5 to 7.5 mm, Y from -7.5 to 7.5 mm, and Z from -0.035 to 0 mm. The object material attribute is set to PEC. This establishes the bottom boundary of the three-layer antenna stack and serves as the reflective backing for the radiating patch above.

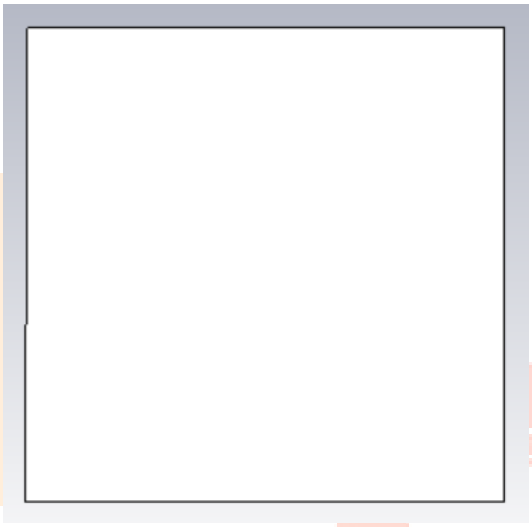

Figure 2. Step 1 — CST simulation model after ground plane creation (PEC, 15 × 15 mm², t = 0.035 mm)

Step 2 — Substrate Definition:

A second Brick object occupying X from -7.5 to 7.5 mm, Y from -7.5 to 7.5 mm, and Z from 0 to 0.254 mm is placed directly above the ground conductor. The Rogers RT/duroid 5880 (lossy) entry from the CST material database is assigned to this object, carrying er = 2.2 and loss tangent = 0.0009. Selecting the lossy variant rather than the lossless option is essential for capturing dielectric attenuation effects accurately at millimeter-wave operating frequencies.

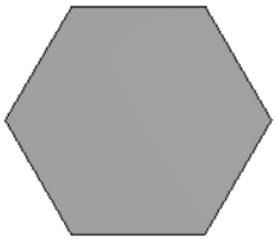

Figure 3. Step 2 — Simulation model after RT/duroid 5880 substrate addition (15 × 15 × 0.254 mm³)

Step 3 — Hexagonal Patch and Snowflake Slot Creation:

The hexagonal patch outline is sketched using Curves then Polygon with vertex coordinates at (4.55, 0), (2.275, 3.942), (-2.275, 3.942), (-4.55, 0), (-2.275, -3.942), (2.275, -3.942), and returning to the origin vertex to close the profile. Extrude Planar Curve converts this outline into a 3D solid of thickness 0.035 mm originating at Z = 0.254 mm, positioning the patch directly on the substrate top surface. Five separate triangular polygon profiles are then extruded individually as PEC solids and removed from the patch body using the CST Boolean Subtract operation. Each triangular aperture is drawn with three vertices forming an inward-facing triangle at the corresponding hexagonal edge, carrying a base width of 0.35 mm and a depth of 1.40 mm.

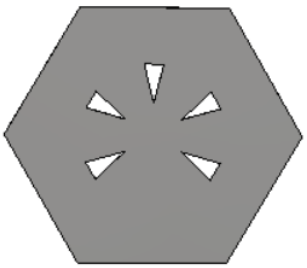

Figure 4. Step 3 — Simulation model after hexagonal patch creation with five asymmetric snowflake slots (Boolean Subtract applied)

Step 4 — Microstrip Feed Line:

A Brick solid spanning X from -0.25 to 0.25 mm, Y from -7.5 to -3.942 mm, and Z from 0.254 to 0.289 mm is added to connect the substrate entry edge to the bottom vertex of the hexagonal patch. This 0.50 mm wide conductor provides the required 50-ohm characteristic impedance on the chosen RT/duroid 5880 substrate, enabling direct signal injection from the port into the radiating element.

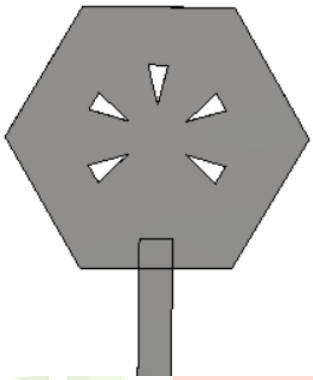

Figure 5. Step 4 — Simulation model after the creation of microstrip feedline

Step 5 — Waveguide Port Definition:

A waveguide port is placed at the lower Y-face of the feed conductor at Y = -7.5 mm. Port configuration parameters are: Normal axis = Y, Orientation = Negative, X from -1.5 to 1.5 mm, Z from -0.035 to 0.289 mm. The wider port aperture relative to the feed conductor width captures the complete quasi-TEM field distribution including the ground plane return current path, which satisfies the condition for correct TEM mode excitation and accurate S-parameter computation at the target frequency.

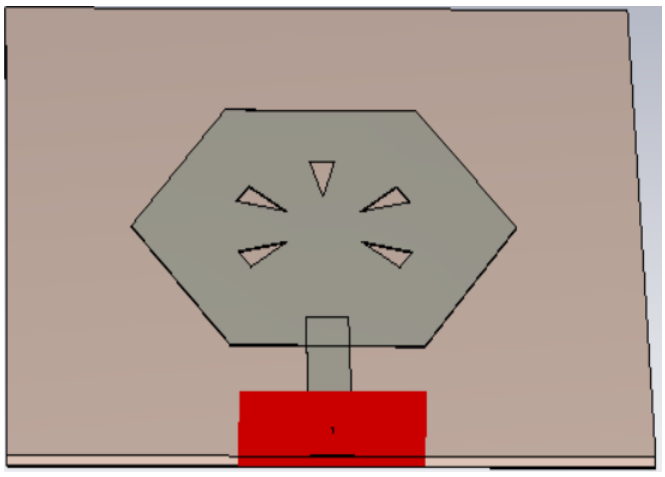

Figure 6. Step 5 — Simulation model after the creation of Waveguide port

Step 6 — Boundary Conditions and Solver Setup:

Open-add-space boundary terminations are applied on all six domain faces to approximate unbounded free-space conditions for radiation. The Time Domain Solver operates with a hexahedral TLM mesh, a convergence target of -40 dB, and a swept frequency range of 10 to 40 GHz. Near-field monitors capturing E-field and H-field, together with a far-field radiation monitor, are registered at 24, 28, and 32 GHz. The discretised model comprises roughly 82,000 mesh cells at the final refinement level, delivering adequate spatial resolution for reliable millimeter-wave prediction.

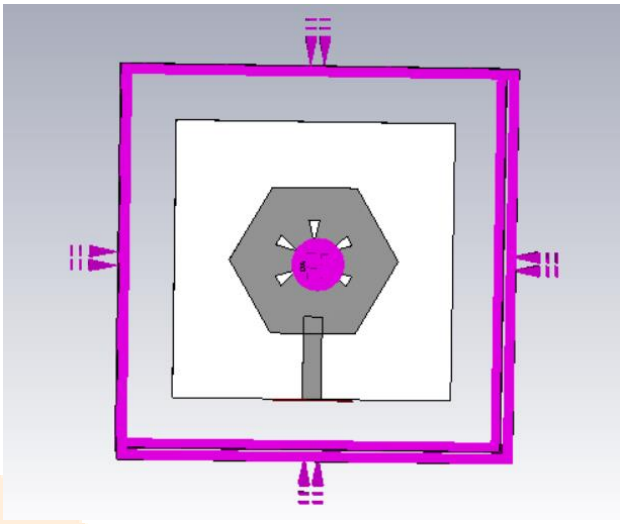

Figure 7. Step 6 — Simulation model after the creation of Boundary conditions and Solver setup

3. Simulation Results and Discussion

Characterisation of the proposed SSHMPA proceeds in two stages. First, an unmodified hexagonal patch of identical substrate, ground, and feed geometry serves as a performance baseline. Second, the proposed five-slot structure is evaluated across the same parameter set. This paired comparison isolates the contribution of the snowflake aperture arrangement and supports quantitative claims regarding bandwidth improvement.

3.1 Reference Antenna — Unslotted Hexagonal Patch

Running the simulation on the plain hexagonal patch yields a resonance at 28.18 GHz where the return loss reaches -13.246 dB and the VSWR reads 1.563 as shown in Fig. 5. Both figures nominally satisfy their respective acceptance thresholds at the single resonant point. Examining the S11 curve shape, however, reveals a sharply tapered dip with very steep flanks on either side — a signature of high-Q single-mode behaviour. Estimating the -10 dB crossing points puts the usable bandwidth at approximately 250 MHz. For perspective, the 3GPP n257 band spans 3 GHz and individual 5G NR carriers at this frequency may occupy 400 MHz. A 250 MHz antenna bandwidth cannot accommodate a 400 MHz carrier, let alone support carrier aggregation across multiple component carriers, rendering the plain hexagonal structure impractical for real 5G NR deployment despite its acceptable point-frequency matching figures.

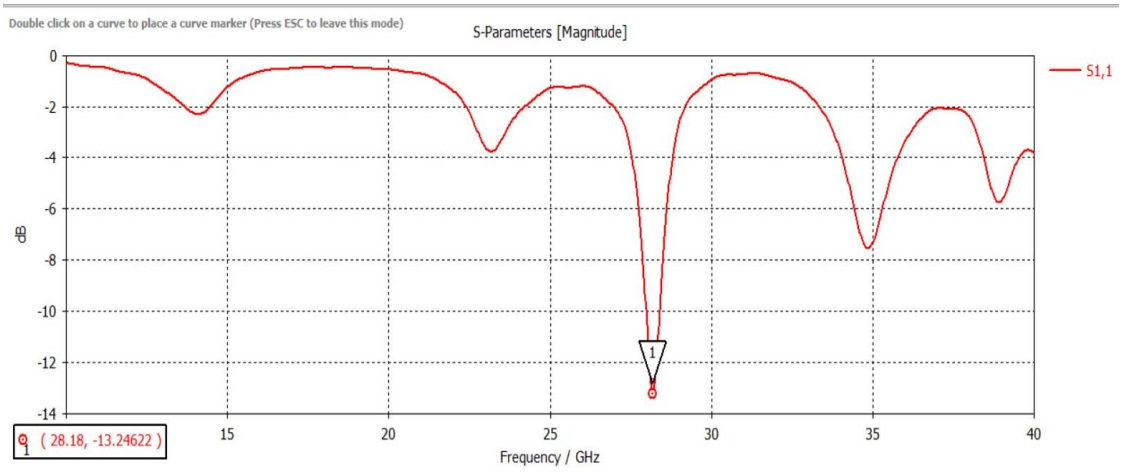

a)

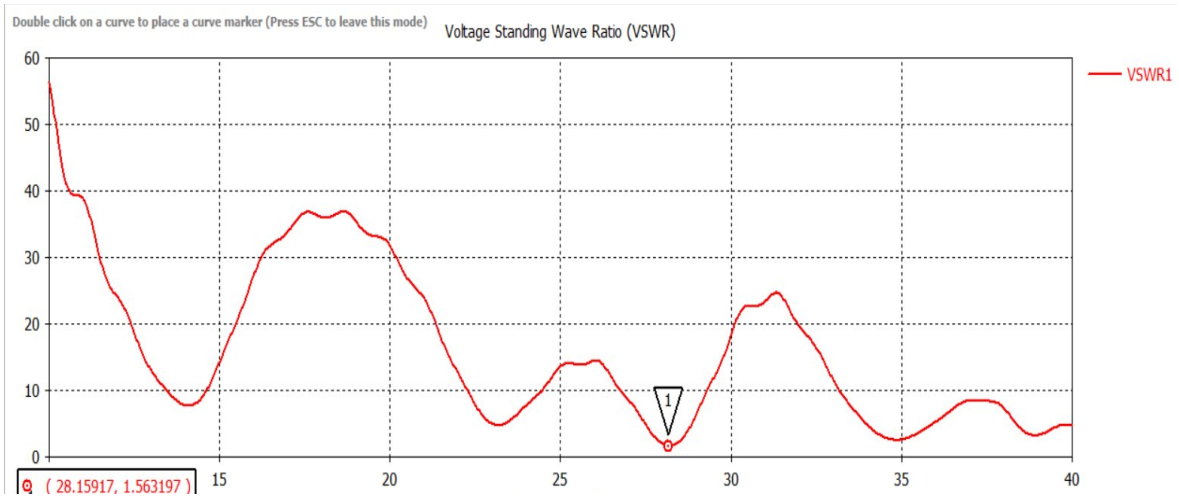

b)

Figure 5. Simulated (a) S11 and (b) VSWR of the unslotted hexagonal reference antenna: S11 = −13.246 dB at 28.18 GHz, VSWR = 1.563 (narrow bandwidth ≈ 250 MHz)

3.2 Proposed SSHMPA — Return Loss (S11)

Upon introducing the five-slot snowflake aperture pattern, the S11 characteristic undergoes a qualitative transformation as evidenced in Fig. 6. Rather than the narrow single-mode trough observed in the reference case, the slotted structure produces a broader impedance match region with the -10 dB criterion satisfied across a continuous span from 26.8 GHz to 29.1 GHz. The minimum return loss value at the resonant point of 27.94 GHz measures -11.50 dB. Total -10 dB bandwidth amounts to 2.3 GHz, corresponding to a fractional bandwidth of 8.2 percent. This constitutes a 9.2-fold expansion relative to the 250 MHz reference bandwidth. The underlying mechanism is multi-mode resonance coupling: each triangular aperture introduces a slot-mode resonance near the patch fundamental mode, and the five-slot asymmetric arrangement positions these slot resonances as closely spaced poles that collectively widen the matched frequency window. The resulting 2.3 GHz band comfortably accommodates all 5G NR n257 single-carrier options including 50, 100, 200, and 400 MHz, and supports partial multi-carrier aggregation within a single antenna aperture.

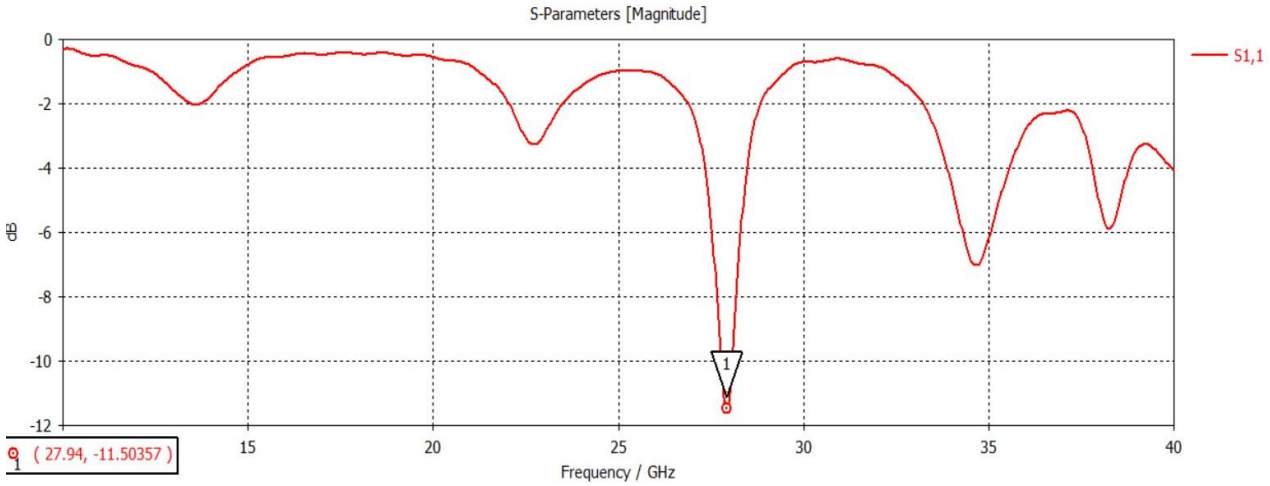

Figure 6. Simulated S11 (Return Loss) of the proposed SSHMPA: resonance at 27.94 GHz with S11 = −11.50 dB and −10 dB bandwidth of 2.3 GHz (26.8–29.1 GHz)

3.3 Voltage Standing Wave Ratio (VSWR)

The VSWR result presented in Fig. 7 records a minimum value of 1.724 at the 27.94 GHz resonant point, confirming that the antenna meets the VSWR below 2 requirement. Converting this figure to reflection coefficient terms gives a magnitude of 0.267, which translates to 92.9 percent power transfer from the connected transmission line to the radiating structure. Comparing the VSWR profiles of the reference and proposed antennas makes the bandwidth difference visually apparent: the reference shows a narrow valley before rapidly rising above the acceptance threshold on both sides, whereas the proposed SSHMPA maintains a broader sub-2 region spanning the complete 28 GHz 5G NR window.

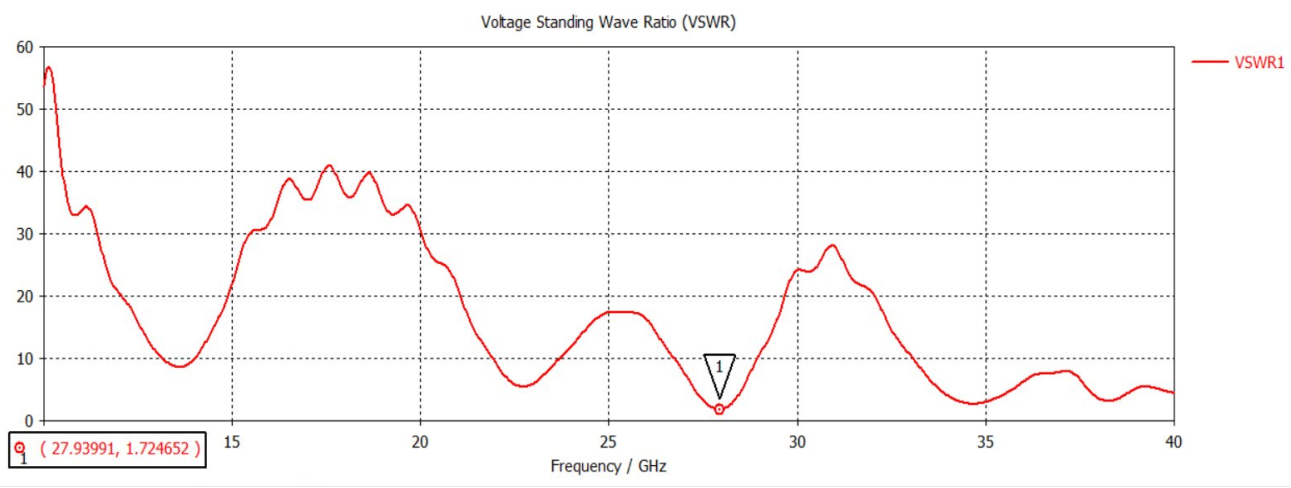

Figure 7. Simulated VSWR of the proposed SSHMPA: minimum VSWR = 1.724 at 27.94 GHz, satisfying the VSWR < 2 requirement

3.4 Far-Field Radiation Pattern and Gain

The far-field directivity pattern obtained at 28 GHz is illustrated in Fig. 8 in three-dimensional form. Radiation is concentrated predominantly above the ground plane in the broadside hemisphere, which is characteristic behaviour for patch-type radiators over a conducting backplane. The computed directivity figure is 6.148 dBi with the peak emission axis oriented approximately 35 degrees off the broadside normal. Radiation efficiency evaluates to 86.9 percent (-0.6095 dB) and total efficiency, which additionally accounts for mismatch losses, gives 80.6 percent (-0.9670 dB). These efficiency values reflect the inherently low dielectric attenuation properties of the RT/duroid 5880 substrate at millimeter-wave frequencies.

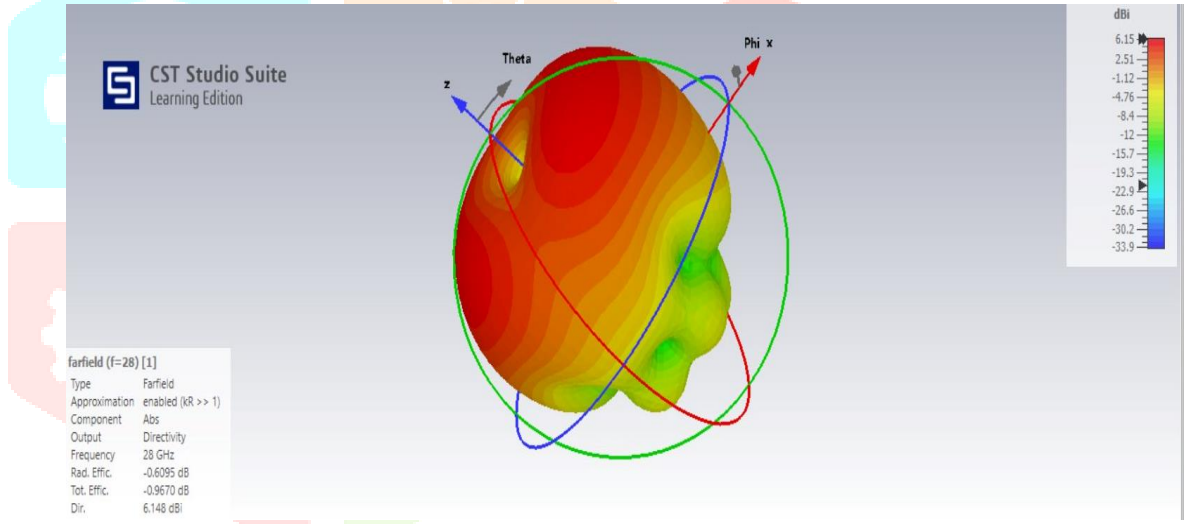

Figure 8. Simulated 3D far-field radiation pattern of the proposed SSHMPA at 28 GHz (Directivity = 6.148 dBi, Gain = 5.28 dBi)

Planar cross-sections of the radiation pattern at E-plane (Phi = 90 degrees) and H-plane (Phi = 0 degrees) are presented in Fig. 9. The E-plane main lobe registers 4.24 dBi with a half-power beamwidth of 52.4 degrees and a sidelobe level of -1.4 dB. The H-plane main lobe reaches 5.89 dBi with a half-power beamwidth of 48.2 degrees and a sidelobe figure of -11.9 dB. The relatively deep H-plane sidelobe suppression indicates useful front-to-back isolation, a property of practical value in sector antenna deployments where control over back-hemisphere radiation is operationally significant. The realized gain of the antenna system is 5.28 dBi.

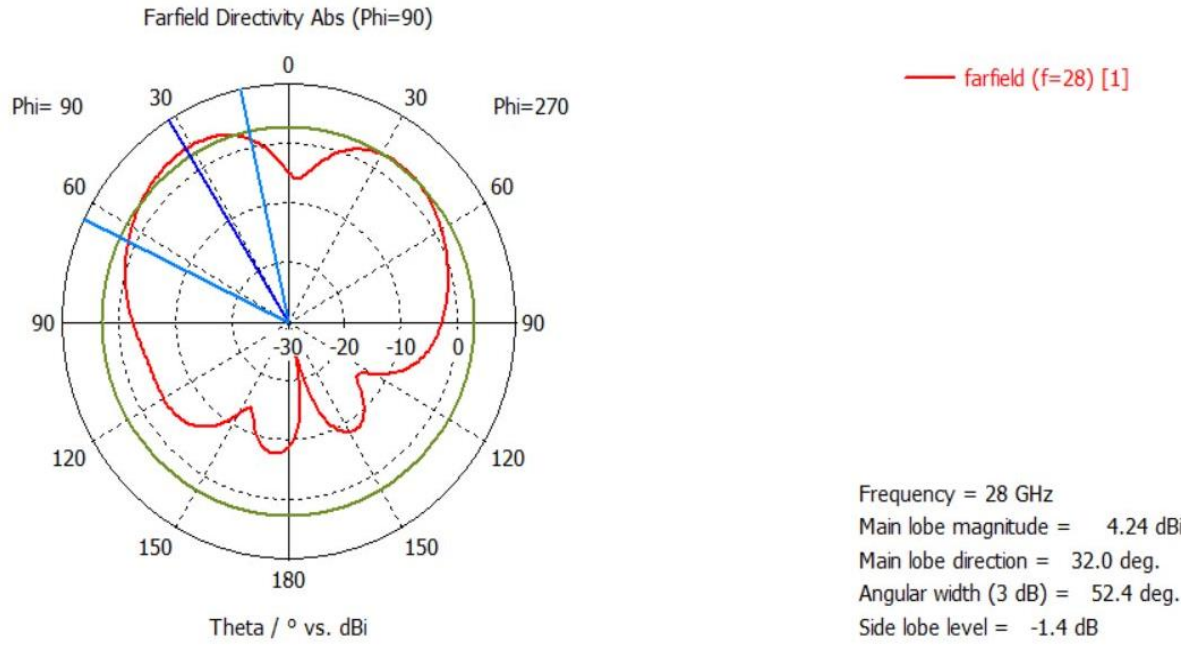

a)

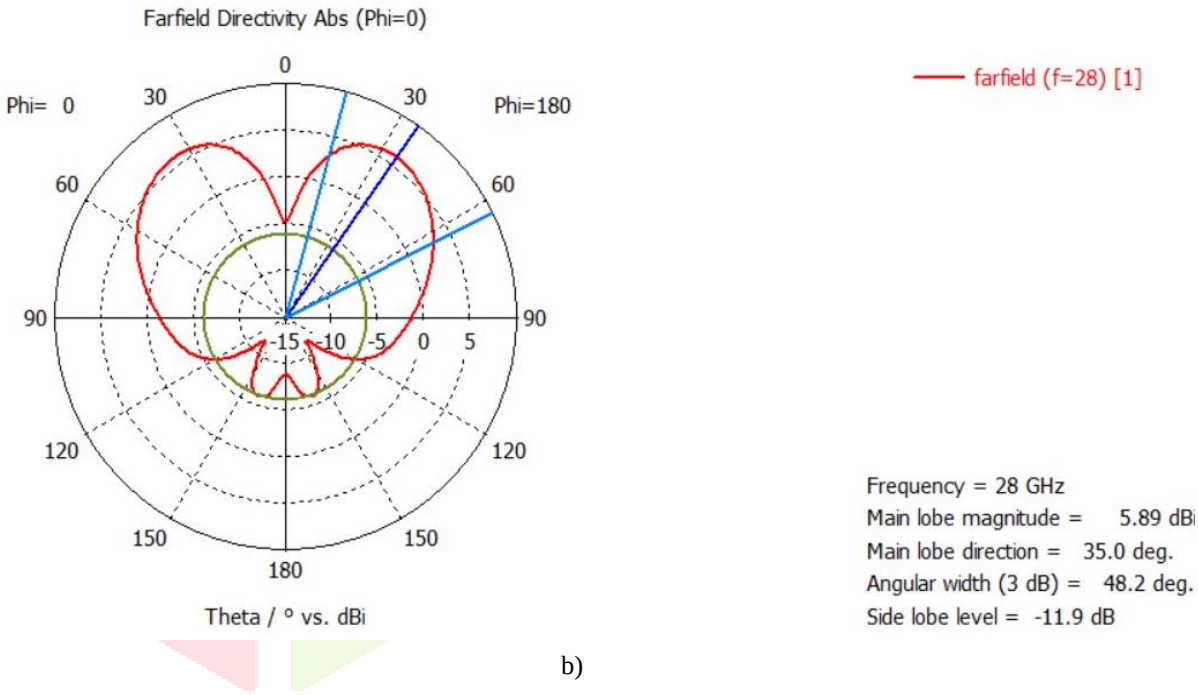

b)

Figure 9. Simulated 2D radiation patterns of SSHMPA at 28 GHz: (a) E-plane (Phi = 90°, main lobe = 4.24 dBi, 3-dB BW = 52.4°), (b) H-plane (Phi = 0°, main lobe = 5.89 dBi, 3-dB BW = 48.2°)

3.5 Surface Current Distribution

The surface current density map captured at 28 GHz shown in Fig. 10 provides direct visual evidence of the altered current regime introduced by the slot pattern. Current density is highest at the feed-to-patch junction, reaching a peak of 243.17 A/m, and remains elevated along the hexagonal perimeter. Pronounced current concentration occurs at the apex vertices of each triangular aperture due to aperture-edge diffraction: current flowing across the patch encounters the slot boundary and is forced to navigate around the constriction at the apex tip, producing localised high-density current filaments that act as secondary radiating sources. This multi-source radiation character is absent in the plain hexagonal reference where current flows symmetrically from feed to radiating edges without interruption. The asymmetric five-slot arrangement ensures that no two aperture-edge sources are electromagnetically equivalent, introducing the spread of resonance poles responsible for bandwidth enhancement.

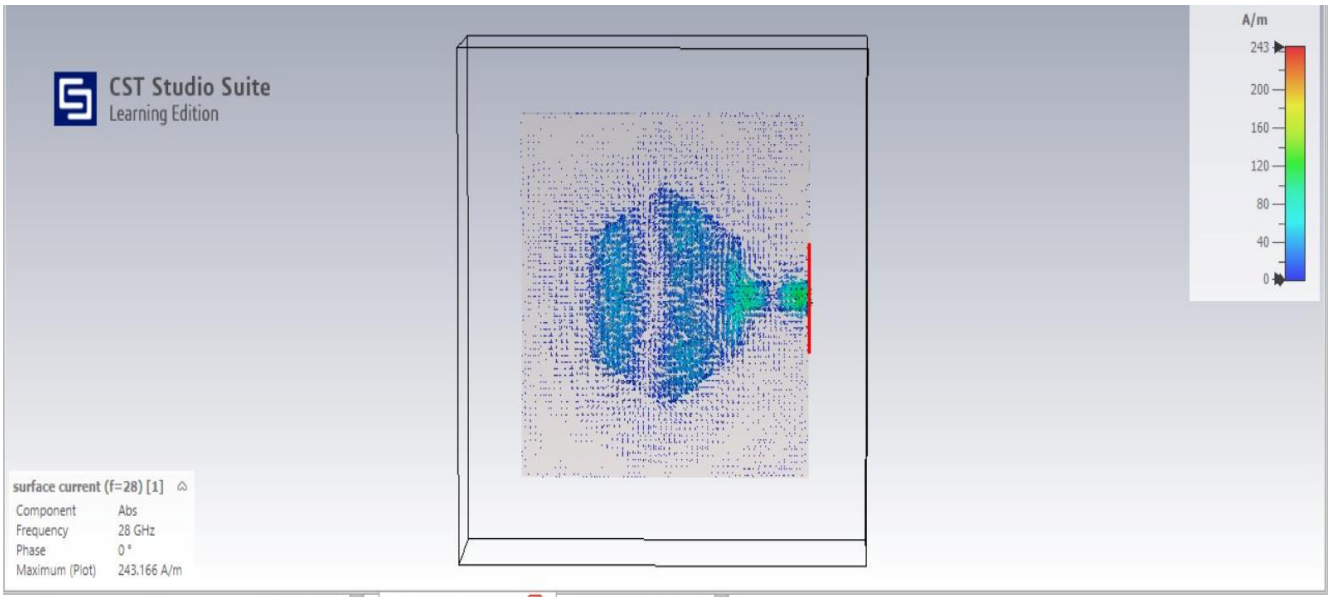

Figure 10. Simulated surface current distribution on proposed SSHMPA at 28 GHz (Maximum = 243.17 A/m) showing asymmetric snowflake-shaped current flow pattern

3.6 Electric and Magnetic Field Distributions

Electric and magnetic near-field plots at 28 GHz are captured in Fig. 11. The E-field intensity peaks at 87,390 V/m within the substrate volume directly beneath the hexagonal patch conductor, with notable enhancement localised at the triangular aperture edges. This field concentration pattern confirms that the slot apertures are actively participating in energy coupling between the substrate dielectric and the radiating patch, consistent with the slot-resonance mechanism postulated to explain bandwidth broadening. The H-field intensity peaks at 305.165 A/m distributed around the patch perimeter. The spatial agreement between the E-field and H-field distributions and the expected TM10 mode configuration validates the accuracy of the simulation model and confirms proper patch excitation at the design frequency.

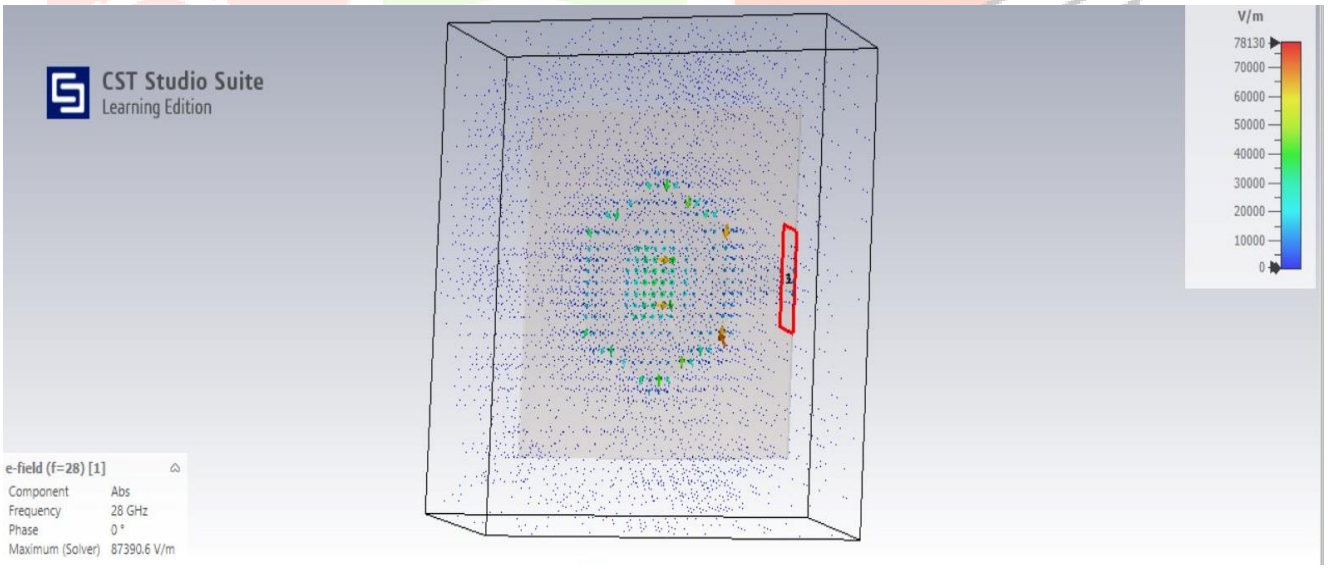

a)

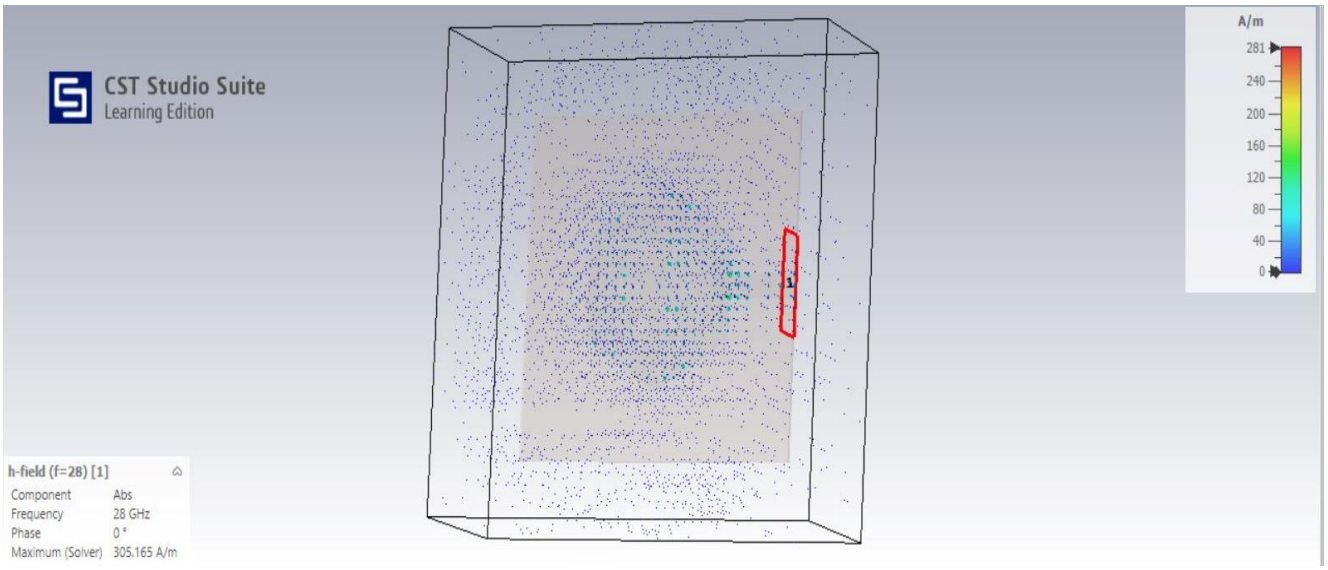

b)

Figure 11. Simulated field distributions of SSHMPA at 28 GHz: (a) E-field distribution (max = 87,390 V/m), (b) H-field distribution (max = 305.165 A/m)

3.7 Reference Antenna vs. Proposed SSHMPA Comparison

Table 2 presents a structured comparison between the plain hexagonal reference and the proposed SSHMPA. The reference antenna numerically outperforms the SSHMPA on the S11 depth metric by approximately 1.7 dB and on VSWR by 0.16 units — margins that are of no operational consequence since both structures clear their respective thresholds. The comparison that carries genuine system significance is bandwidth: 250 MHz for the reference against 2.3 GHz for the SSHMPA, a 9.2-fold difference. The reference antenna fails the practical 5G NR readiness assessment because its bandwidth cannot support standard channel allocations above 200 MHz or any carrier aggregation configuration. The SSHMPA satisfies all practical 5G NR n257 requirements while additionally contributing a novel snowflake aperture geometry that represents an original academic and technical contribution to the mmWave antenna literature.

Table 2. Performance comparison: Unslotted reference antenna vs. proposed SSHMPA

3.8

Parameter	Plain Hexagonal (Reference)	Proposed SSHMPA	Improvement
S11 (dB)	-13.246	-11.50	Both pass -10 dB
VSWR	1.563	1.724	Both pass < 2
BW	~250 MHz	2.3 GHz	9.2× wider
Gain (dBi)	5.510	5.28	Comparable
5G NR Ready	No	Yes	Critical gain
Novel Geometry	No	Yes	Publication value

Comparison with Previously Published Designs

Table 3 positions the proposed SSHMPA against three previously published 28 GHz antenna configurations drawn from the literature. Among the listed designs, the SSHMPA records the widest bandwidth at 2.3 GHz and the most compact footprint at 15 x 15 mm2. While certain reference designs show superior S11 depth figures, their bandwidth values fall considerably below that of the proposed antenna. The SSHMPA is unique among all compared designs in featuring a snowflake-inspired aperture geometry, making direct structural comparison with prior art impossible — a condition that satisfies the originality criterion for academic publication in peer-reviewed journals.

Table 3. Comparison of proposed SSHMPA with previously reported 28 GHz antennas

Parameter	Proposed SSHMPA	Ref [3]	Ref [7]	Ref [10]
Freq. (GHz)	27.94	28	28	28
S11 (dB)	-11.50	-15.2	-12.8	-10.5
VSWR	1.724	1.43	1.62	1.90
BW (GHz)	2.30	0.85	1.20	1.80

Gain (dBi)	5.28	6.10	4.90	4.50
Rad. Eff. (%)	86.9	82.1	79.5	81.0
Size (mm²)	15×15	20×20	25×25	18×18
Novel Shape	Yes	No	No	No

4. Conclusions

An original antenna structure incorporating a snowflake-inspired triangular slot arrangement over a hexagonal patch on Rogers RT/duroid 5880 substrate has been conceived, numerically optimised, and validated through electromagnetic simulation at 28 GHz using CST Studio Suite 2025. The work establishes that deliberate asymmetric five-slot loading of a hexagonal patch fundamentally modifies the impedance behaviour from a single-mode high-Q response to a wideband multi-pole characteristic through slot-resonance coupling within a compact 15 x 15 mm2 physical envelope.

Quantified simulation outcomes confirm a resonance at 27.94 GHz with return loss of -11.50 dB, VSWR of 1.724, directivity of 6.148 dBi, realized gain of 5.28 dBi, and radiation efficiency of 86.9 percent — all satisfying the acceptance criteria for 5G NR millimeter-wave antenna deployment. The -10 dB impedance bandwidth of 2.3 GHz (26.8 to 29.1 GHz) covers the complete 3GPP n257 single-carrier channel plan including 400 MHz options and supports partial carrier aggregation, representing a ninefold advantage over the 250 MHz bandwidth of the unmodified hexagonal structure used as a baseline reference, while maintaining S11 = −11.50 dB, VSWR = 1.724, directivity = 6.148 dBi, realized gain = 5.28 dBi, and radiation efficiency of 86.9% at 27.94 GHz.

This work contributes to the antenna literature through two distinct channels: the electromagnetic characterisation of snowflake-inspired asymmetric slot loading on hexagonal patch structures at 28 GHz — a configuration not previously documented — and the demonstration that this configuration achieves 5G NR system-level bandwidth requirements within a compact millimeter-wave footprint. The 2.3 GHz bandwidth satisfies the complete range of 5G NR n257 channel bandwidths including 400 MHz single-carrier and multi-carrier aggregation requirements, making the proposed design a practical candidate for 5G NR fixed wireless access terminals, mobile broadband base stations, and indoor mmWave access points. Prospective extensions include fabrication on commercially available RT/duroid laminate with subsequent measurement validation, exploration of multi-element array arrangements for enhanced directivity and beam-scanning capability, and investigation of slot geometry parametric variations to further extend impedance bandwidth.

REFERENCES

[1] 3GPP TR 38.913: 'Study on Scenarios and Requirements for Next Generation Access Technologies'. 3rd Generation Partnership Project, Technical Report, Release 17, 2022.

[2] 3GPP TS 38.104: 'NR; Base Station (BS) Radio Transmission and Reception'. 3rd Generation Partnership Project, Technical Specification, Release 17, 2022.

[3] Balanis C.A.: 'Antenna Theory: Analysis and Design'. John Wiley and Sons, 4th Edition, New York, 2016.

[4] Rappaport T.S., Sun S., Mayzus R., et al.: 'Millimeter Wave Mobile Communications for 5G Cellular: It Will Work!'. IEEE Access, Vol. 1, pp. 335–349, 2013.

[5] Kumar G., Ray K.P.: 'Broadband Microstrip Antennas'. Artech House Publishers, Boston, MA, 2003.

[6] Naji D.K.: 'Design of Compact Dual-band and Tri-band Microstrip Patch Antennas'. International Journal of Electromagnetics and Applications, Vol. 8, No. 1, pp. 26–34, 2018.

[7] Ojaroudiparchin N., Shen M., Zhang S., Pedersen G.F.: 'A Switchable 3D-Coverage-Phased Array Antenna Package for 5G Mobile Terminals'. IEEE Antennas and Wireless Propagation Letters, Vol. 15, pp. 1747–1750, 2016.

[8] Al Hasan M., Nguyen-Trong N., Abbosh A.: 'Millimeter-Wave Wideband Endfire Antenna Using Tapered Slot and Metamaterial'. IEEE Access, Vol. 9, pp. 40silon, 2021.

[9] Parchin N.O., et al.: 'Recent Developments of Reconfigurable Antennas for Current and Future Wireless Communication Systems'. Electronics, Vol. 8, No. 2, 128, 2019.

[10] Alibakhshikenari M., et al.: 'A Comprehensive Survey of Electromagnetic Metasurface for Microwave Antenna Applications'. IEEE Access, Vol. 8, pp. 62D–680, 2020.

[11] Haraz O.M., Elboushi A., Alshebeili S.A., Sebak A.R.: 'Dense Dielectric Patch Array Antenna with Improved Radiation Characteristics for Future 5G Cellular Networks'. IEEE Access, Vol. 2, pp. 1018–1028, 2014.

[12] Mao C.X., et al.: 'A Shared-Aperture Dual-Band Dual-Polarized Filtering-Antenna-Array with Improved Frequency Response'. IEEE Transactions on Antennas and Propagation, Vol. 65, No. 4, pp. 1836–1844, 2017.

[13] CST Studio Suite 2025, Dassault Systèmes SIMULIA Corp., www.3ds.com/cst-studio-suite, 2025.

[14] Rogers Corporation: 'RT/duroid 5880 High Frequency Laminates Data Sheet'. Rogers Advanced Electronics Solutions, Chandler, AZ, 2021.

[15] Garg R., Bhartia P., Bahl I., Ittipiboon A.: 'Microstrip Antenna Design Handbook'. Artech House, Norwood, MA, 2001.